ORIGINAL ARTICLE

Zingiber officinale powder as a biosorbent for adsorption of acid violet 90 from aqueous solutions

A. Hashem[1] · S. Dubey[2] · Y. C. Sharma[3] · S. Farag[1] · A. A. Aly[1]

Abstract

The potential of *Zingiber officinale* powder was explored as a biosorbent for the uptake of Acid Violet 90 dye from the aqueous solutions. The biosorbent was characterized using FTIR, XRD, SEM, and Zeta potential techniques. The impact of various experimental parameters such as pH, dye concentration, adsorbent dose, contact time, and temperature on the adsorption capacity of biosorbent was investigated using batch adsorption. The *Zingiber officinale* powder showed a dye adsorption efficiency of 342.68 mg/g. The optimum adsorption was achieved at pH 2, adsorbent dose of 0.2 g/L, contact time of 10 min, and 40 mg/L dye concentration at a temperature of 30 °C. The experimental isotherm data was analyzed by two-parameter and three-parameter models and best explained by the Freundlich model. The pseudo-second-order model elucidated the kinetic behavior of the uptake with pore-diffusion as the rate-determining step. The thermodynamic study suggested the uptake of dye was feasible, spontaneous, and exothermic in nature. The results revealed that the *Zingiber officinale* powder has the potential to be used as an adsorbent for the treatment of water.

Keywords *Zingiber officinale* · Kinetics · Isotherm · Thermodynamic · Acid violet 90 dye

1 Introduction

The most essential and leading solvent used in textile industries is water. Textile industries are water-intensive in each of their production steps and thus, consume enormous quantities of water. Water is used mainly as a solvent for chemicals and dyes, as a means to transfer dyes and chemicals to fabric, and also as a cleansing and rinsing medium [1]. Textile factories in India alone consume around 425,000,000 gallons of water daily to produce clothing materials. But, more importantly, these factories release 90–95% of used water as effluents at the end that are frequently dumped direct into nearby waterways [2]. While this being a just a figure, perhaps the larger problem lies in the inconsiderable pollution of water, particularly in the developing countries.

Inadequate facilities for effluent discharge and a lack of strict regulations by governmental organizations have led to water contamination to a vast extent [3]. Textile wastewaters have a wide range of pollutants that contaminate external water bodies. These pollutants include non-biodegradable organics and inorganics such as dyes, metals, surfactants, phenols, pesticides, etc. [4]. Among these, dyes are the most dangerous chemicals that have been adversely affecting the environment. The physico-chemical effects of dyes in water are: (i) increased concentration of total suspended solids (TSS), (ii) elevated levels of biochemical oxygen demand (BOD) and chemical oxygen demand (COD), (iii) high level of total dissolved solids (TDS) (iv) change in pH (v) colored water, and (vi) unpleasant pungent odor [5–7]. Increased levels of COD and BOD in textile effluents lead to the death of many aquatic life due to the depletion of oxygen. Higher TDS and TSS levels block the entry of light, thereby deteriorating water quality and making it unfit for plants and animals' survival. This contamination has also led to increased rates of cancer, respiratory diseases, and skin infections among workers working in textile industries [8, 9].

Acid violet 90 (AV) is an aromatic azo compound that is formed when the aryl diazonium cation is converted to another aryl ring that contains an electron-releasing group

✉ A. Hashem
  alihashem2000@yahoo.com

1   Textile Research and Technology Institute, National Research Centre, Dokki, Cairo, Egypt

2   Department of Chemistry, HNB Garhwal University, Garhwal, Srinagar 246174, India

3   Indian Institute of Technology (Banaras Hindu University), Varanasi, India

[10]. The diazonium salts are more stable when the coupling reactions are carried out at lower temperatures. Azo dyes derived from oxidation of hydrazines and benzidines are carcinogenic, and mutagenic and lead to severe human organ damage [11, 12]. These dyes are metal-complex dyes formed by the combination of a metal ion (usually chromium, nickel, cobalt, iron, and copper) with a single or double dye molecules. The high water-solubility of these dyes makes their removal quite difficult [13]. Therefore, azo dye pollution is a serious problem that needs to be addressed urgently [14, 15]. Several methods have been employed to remove azo dyes from effluents but these are outdated, cost-ineffective, generate excess toxic sludge, have high maintenance costs, huge energy, and reagent requirements, and often lead to incomplete removal of contaminants, etc.

Adsorption is a widely used technique which is a more rapid and efficient process and also has the ability to remove a wide range of organic and inorganic compounds from water [16–19]. However, the high cost of chemical adsorbents and the amount of toxic substances they release has encouraged researchers to find viable alternatives that are cheaper, natural, biodegradable, biocompatible, and less harmful.

Bio-adsorbents are non-conventional adsorbents derived from biological materials for the effective removal of organic and inorganic pollutants from water. For dye removal various biosorbents have been used so far such as wheat flour, Graham flour, cellulose, *Penaeus indicus* shrimps, *Ganoderma lucidum, Spirulina platensis*, etc. [20]. Based on this rationale, in this work, we reported the adsorption properties of *Zingiber officinale* powder for the removal of acid violet 90 dye from aqueous solutions. Ginger (*Zingiber officinale*) belongs to the family of Zingiberaceae and is the most commonly consumed dietary condiments in the world [21]. It is also widely used as a traditional herbal medicine and an additive to enhance the taste of food. India is the largest producer of ginger with its production greater than 275,000 million tonnes per year [22]. Due to its worldwide and substantial availability, its various parts are used extensively in the research field such as its extract

containing several water-soluble phyto-constituents is used for synthesizing nanoparticles viz., AgNPs [23], and its treated waste material is used as a biosorbent for removal of dyes [22, 24–26]. In this regard, we investigated the ginger powder for the treatment of water containing AV 90 dye. The novelty of this work is that based on the perusal of literaturethere is no study has been reported for the removal of AV 90 dye with ginger root powder. The effects of various experimental parameters such as pH of the solution, initial concentration of dye, contact time, and temperature on the uptake process were investigated through the batch process of adsorption. The non-linear regression method was used to determine the most appropriate isotherm and kinetic models for this system.

2 Materials and methods

2.1 Materials

Zingiber officinale (ginger) was obtained from the local vegetable shop. Acid violet 90 (AV) was supplied from Synthesia Company Czech Republic and was not purified prior to use. All other chemicals such as sodium hydroxide, sodium carbonate, nitric acid, HCl, ethyl alcohol, and acetone were all laboratory-grade chemicals (Merck, Germany) and used as received (Table 1).

2.2 Preparation of Zingiber officinale biosorbent

Ginger (*Zingiber officinale*) rhizomes/roots were washed several times with distilled water to get rid of any impurities stuck to the roots. The outer thick layer of the rhizomes was removed and was grated with a grater to obtain rhizomes in the form of flakes. The ginger flakes thus obtained were placed on a glass plate and covered with gauze to prevent any sort of contamination. The ginger flakes containing glass plates were kept under natural sunlight for complete dryness. After about three weeks, the ginger flakes get dried completely. The ginger flakes were ground to obtain a

Table 1 Chemicals used for adsorption of AV 90 dye onto *Zingiber officinale* biosorbent

Chemicals used	Chemical formula	Molecular weight (g/mol)	Source	Purity %
Acid Violet 90	$C_{40}H_{27}CrN_8O_{10}S_2.2Na$	944.8	SynthesiaCompany, Czech Republic	98.5
Sodium Hydroxide	NaOH	40	Merck, Germany	≥ 97.0
Sodium Carbonate	Na_2CO_3	105.99	Merck, Germany	99.99
Nitric Acid	HNO_3	63.01	Merck, Germany	65.0
Hydrochloric Acid	HCl	36.485	Merck, Germany	37.0
Ethyl Alcohol	C_2H_5OH	46.07	Merck, Germany	99.9
Acetone	C_3H_6O	58.08	Merck, Germany	99.9

powder with different molecular sizes. The ground sample was screened through different size sieves to separate granulates and particles with a size range of 50–125 μm were separated. The root powder was mixed with an excess quantity of distilled water (1:10) under vigorous stirring at 60 °C for 30 min. The extracts were cooled, filtered by Whatman No.1 filter paper to remove the soluble extract, and stored at room temperature for experimental use.

2.3 Characterization of prepared Zingiber officinale biosorbent

The X-ray diffraction (XRD) pattern of the prepared biosorbent was measured in the continuous scanning mode on PANalytical diffractometer system (X'Pert PRO) using Cu K radiation ($\lambda = 1.5406$ A^0) in the 2θ range of 2^0 to 60°. To determine the vibrational frequencies of the functional groups attached to the surface of the biosorbent, Fourier transform infrared (FTIR) spectra was recorded on a Perkin–Elmer Spectrum 1000 spectrophotometer over 4000–400 cm^{-1} using the KBr disk technique. The BET surface area, total pore volume, and average pore radius were measured using the Brunauer-Emmett-Teller (BET) method. The pore size distributions of the samples were obtained by using the Barrett-Joyner-Halenda (BJH) method(QuantachromeTouchWin) (Table 2). To investigate the surface morphological as well as elemental analysis of the prepared biosorbent, scanning electron microscopy (SEM) and energy-dispersive X-ray spectroscopy (EDS) analysis was performed using Scanning Electron Microscope (JEOL-JSM-5600). The point of zero charges (pH$_{pzc}$) of the biosorbent was evaluated as follows:100 ml of 0.01N NaCl solutions were prepared and added to eleven (11) different Erlenmeyer flasks. The pH values of the flasks were respectively tuned(from pH 2.0 to pH 12.0) using either 0.01N HCl or 0.01N NaOH solution. The initial pH of the solutions was measured with a pH meter and noted as pH initial. After the constant value of pH initial had been reached, 0.1 g of adsorbent sample was added to each Erlenmeyer flask. The solution pH was measured after 24 h and noted as pH final. Then, a plot of the change in pH, ΔpH (pHfinal-pHinitial)against pH

Table 2 Physical parameters of *Zingiber officinale* biosorbent

Element content (%)				
C	O	K	Ca	Mg
59.95	37.77	1.32	0.55	0.42
Physical characteristics				
BET Surface Area (m^2/g)				39.5942
Total Pore Volume (cc/g)				2.7015e-002
Average Pore Radius (nm)				1.3646e+000

initial was generated and the pHpzc of the sample was marked off at the point where the ΔpH is zero.

2.4 Batch adsorption experiment

The stock solution of AV 90 dye was prepared by dissolving the requisite amount of dye in distilled water. The solutions of the required concentrations were prepared by dilution of the stock solution with their pH maintained. In an equilibrium experiment, a certain amount (0.02 g) of *Zingiber* powder and 100 ml of AV 90 solution were placed in a 125 ml glass stoppered flask and stirred in a thermostatic shaker operated at 200 rpm at 30 °C for a pre-defined time. After experiments, the flasks containing samples were withdrawn from the shaker and centrifuged to separate the biosorbent from the solution. The residual concentration of the supernatant solution was measured with a Shimadzu UV/Visible Spectrophotometer. The equilibrium adsorption capacity of dye adsorbed onto adsorbent, q$_e$ (mg/g), and percent removal of dye were calculated by the following relationships:

$$q_e \frac{(C_o - C_e).V(l)}{W} \tag{1}$$

$$\text{Removal\%} = \frac{C_o - C_e}{C_o} x100\% \tag{2}$$

where C_o and C_e are the initial and final concentrations of AV 90 (mg/L), V is the volume (L) of dye, and W(g) is the weight of the adsorbent. All adsorption experiments were carried out in duplicate and the corresponding mean values were reported.
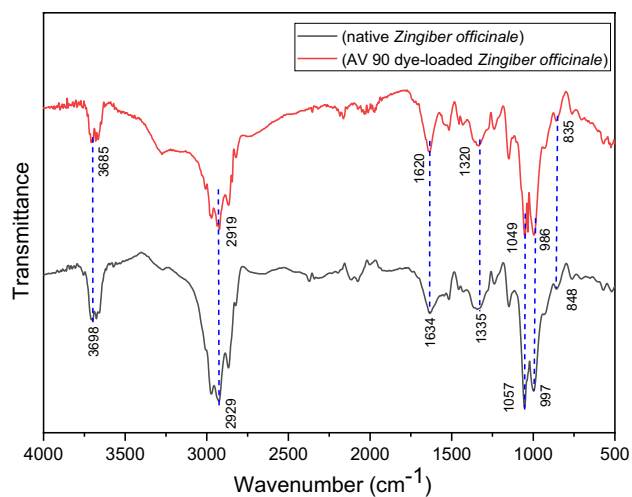
3 Results and discussion

3.1 Structural and morphological characterization of Zingiber officinalebiosorbent

The presence of various functional groups attached to the surface of native biosorbent prior to the adsorption and post-adsorption was investigated using FT-IR and the corresponding spectrum is presented in Fig. 1. The band at region 3000–3500 cm^{-1} represents the O−H stretching vibration of the glucose molecule in the cellulose structure. This group is responsible for the formation of either intra- or inter-molecular hydrogen bonds, based on their linkage alignment within the glucose molecule. The native *Zingiber officinale* sample exhibited an absorption peak at 3269 cm^{-1}, indicating the presence of bonded and free hydroxyl groups, due to the O–H groups' vibrations (carboxylic acid, phenol, or alcohols) of cellulose, lignin, hemicellulose, and adsorbed water [27]. The peak at 2929 cm^{-1} is associated with the

Fig. 1 FTIR of **A** native *Zingiber officinale*, **B** AV 90 dye-loaded *Zingiber officinale*

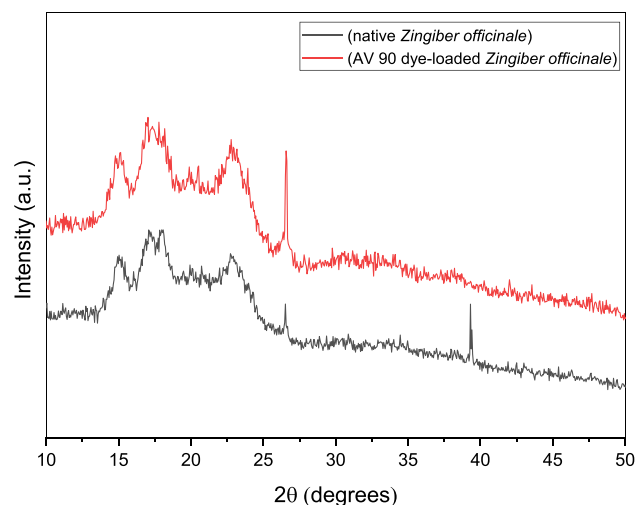**Fig. 2** XRD diffractogram of *native Zingiber officinale* and AV 90 dye-loaded *Zingiber officinale*

stretching vibration of the C–H groups [19]. The dual bands at 1634 and 1335 cm^{-1} correspond to the CH$_2$ stretching of an aromatic ring from the hemicellulose and O-H group from phenolic compounds. The peak at 1057 cm^{-1} indicates the stretching vibration of C−O groups attributed to carboxylic acid, alcoholic, phenolic, ether, and ester groups of lignin and hemicelluloses components [19]. The minute peak at 848 cm^{-1} is due to the bending vibration of =C–H groups present on the surface of the *Zingiber officinale* biosorbent [22, 25, 26, 28].

After the uptake of AV 90 dye, a minor shift in the peaks 3906 to 3935, 3869 to 3896, 3839 to 3844, 3824 to 3793, 3804 to 3761, 3755 to 3703, 3698 to 3666, 1634 to 1620, and 1335 to 1320 cm^{-1}. The slight difference between the pre-and post-biosorption wavenumbers is a consequence of the adsorptive interaction between the acid violet 90 dye molecules and the *Zingiber officinale* surface [29, 30].

The X-ray diffraction spectra of native *Zingiber officinale* granules before and after adsorption of Acid violet 90 dye are presented in Fig. 2. The XRD of native *Zingiber officinale* granules shows characteristic crystallinity peaks of an A-type pattern. The native Zingiber granules had a semi-crystalline structure with sharp diffraction peaks at 15.07°, 17.16, 18.05°, 22.88°, 26.52°, and 39.34° (2θ), which indicated a typical pattern like starch A-type [31–33]. The degree of crystallinity was 44%. The inter- and intra-molecular hydrogen bonds were responsible for the crystalline structure [34]. As can be seen in Fig. 2, native Zingiber granules dyed with acid violet 90 showed a similar profile to native ones, but the diffraction peaks at 17.16 and 22.88 were split in addition to a disappearance of the diffraction peak at 39.30° (2θ).

For the topographical aspect of the biosorbent before and after adsorption, electron microscopic (SEM) analysis was

carried out and the corresponding micrographs have been presented in Fig. 3. The SEM pictures of native *Zingiber officinale* biosorbent revealed the irregular and rough surface having prominent pores. These pores get filled with the AV 90 dye molecules upon uptake from the solution displaying the adherence of dye molecules on the surface of the *Zingiber officinale* biosorbent. On comparing the EDX spectra of the biosorbent before and after the uptake process (Fig. 4), the presence of new peaks for the elements S and Cr that are the constituents of the AV 90 dye confirmed the adsorption of dye molecules over the surface of *Zingiber officinale* biosorbent.

The determination of pH$_{zpc}$ is helpful in the evaluation of the nature of the adsorbent surface and the adsorption of contaminants over the surface as pH >pH$_{zpc}$ favors the uptake of cationic species and the reverse favors the anionic species from the aqueous medium. The pH$_{zpc}$ of the *Zingiber officinale* biosorbent was found as 7.8 (figure not shown).
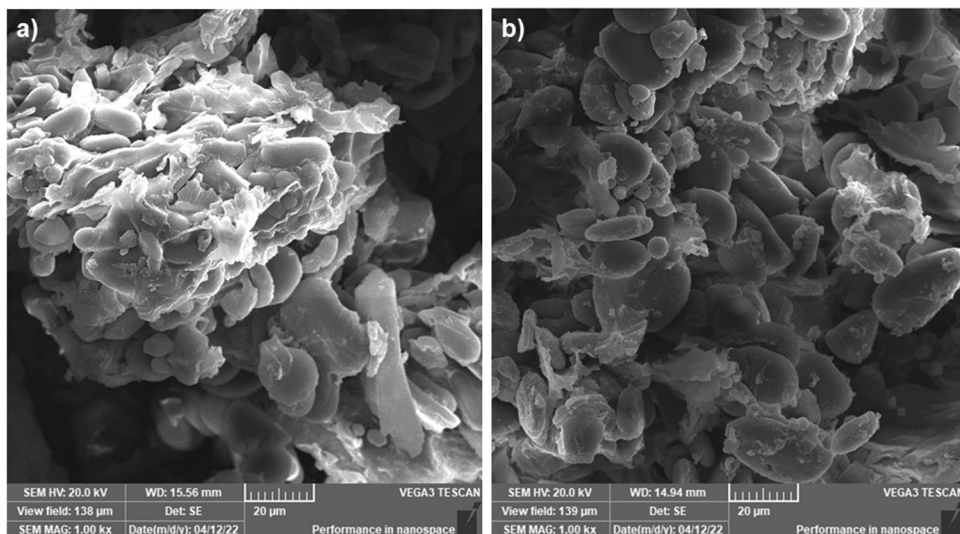
3.2 Application of Zingiber officinale biosorbent for adsorption of acid violet

The prepared *Zingiber officinale* biosorbent was employed for the removal of AV 90 dye from the aqueous solutions and the effect of various parameters governing the adsorption process is investigated and discussed in detail in the subsequent sections.

3.2.1 Effect of initial pH on adsorption capacity

The aqueous chemistry (i.e., the surface charge of adsorbate and adsorbent, degree of ionization of adsorbate in the solution, and dissociation of functional groups present

Fig. 3 SEM images of **a** native and **b** AV 90 dye-loaded *Zingibero fficinale* biosorbent

Fig. 4 EDX images of **a** native and **b** AV 90 dye-loaded *Zingiber officinale* biosorbent

Biomass Conversion and Biorefinery
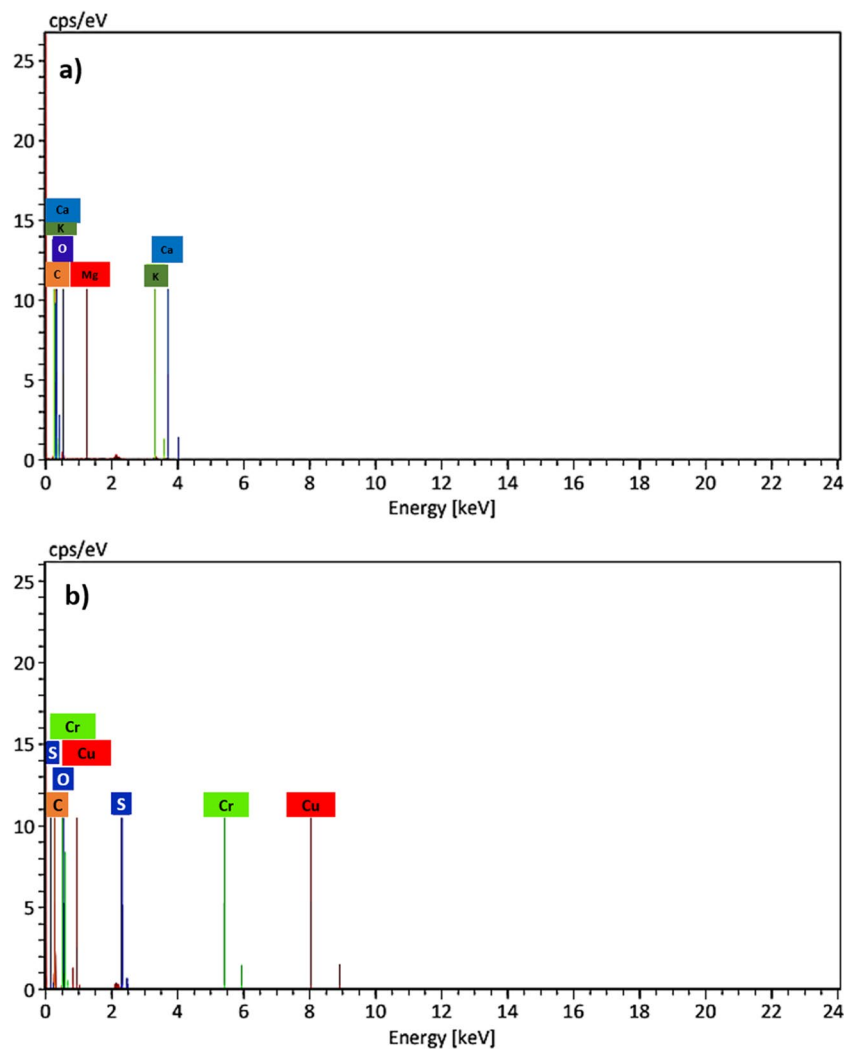
on the adsorbent surface) and the binding capacity of the adsorbent towards the adsorbate is entirely governed by the pH of the solution. Thus, solution pH plays an important role in any adsorption process. The effect of pH was studied by conducting the experiment with 100 mL of initial AV concentration of 30 mg/L, adsorbent dose of 0.2 g/L, contact time of 2 h, and varying pH from 2.0 to 10.0 at the temperature of 30 °C. The effect of the initial solution pH on the adsorption of AV is shown in Fig. 5.

The result showed that higher adsorption capacity was recorded at acidic pH. Meanwhile, the adsorption capacity progressively abated with a decrease in the acidity of the adsorbate solution This observation is explained by the fact that at decreasing acidity, the electrostatic repulsion between the anionic character of the Acid violet 90 dye and those on the adsorbent surface [35, 36].

It is evident from the figure that the amount of dye adsorbed on the surface of the Zingiber biosorbent declined with the elevation in the pH of the solution. This behavior can be explained by taking into account the pH_{zpc} of the adsorbent as well as the solution pH. At lower solution pH ($pH < pH_{zpc}$) the surface of the adsorbent would be positively charged due to the protonation of surface hydroxyl groups facilitating the dye adsorption due to electrostatic attraction between the dye molecules and the biosorbent. However, when the pH of the solution increases ($pH > pH_{zpc}$) the adsorbent surface become negatively charged, and thus the adsorption of AV which is an anionic dye diminished resulting in a decline in the adsorption rate [37, 38]. As the adsorption was maximum at pH 2.0 hence it was regarded as an optimum pH and all experiments were carried out by maintaining this pH.

3.2.2 Effect of adsorbent dose on adsorption capacity

The amount of adsorbent is another important parameter that affects the adsorption process. To assess the effect of the adsorbent dose on the adsorption of AV, the experiment was

Fig. 5 Effect of pH on adsorption capacity of *Zingiber officinale* biosorbent for AV 90 dye (reaction conditions: dye conc.=30 mg/l; adsorbent conc.= 0.2 g/L; contact time =2h; temperature= 30 °C; particle size range= 50−125 μm)
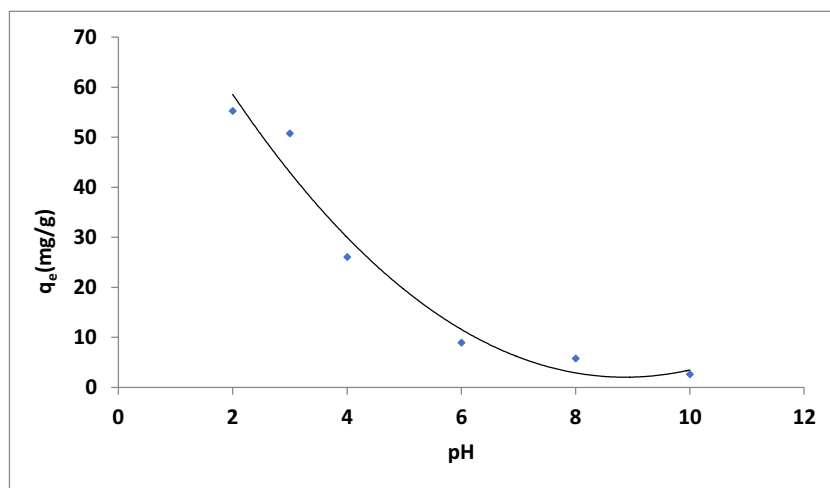
Fig. 6 Effect of adsorbent dose on adsorption capacity of *Zingiber officinale* biosorbent for AV 90 dye (reaction conditions: dye conc.= 30 mg/L; pH = 2; contact time =2h; temperature= 30 °C; particle size range= 50−125 μm)

🍏 Springer
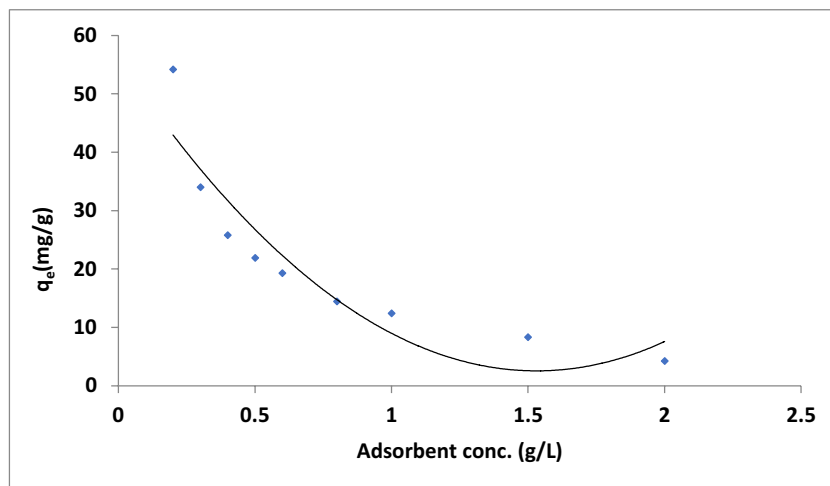
conducted by varying the dose from 0.2 to 2 g/L and keeping other experimental conditions constant (Fig. 6).

The figure shows that the dye uptake decreases with an increase in adsorbent concentration. At lower concentrations of adsorbent, the number of active sites available on the surface is higher while an increase in concentration leads to the filling up of the pores of the adsorbent leading to aggregation of particles and thereby decreasing the available surface area for dye uptake. The optimum adsorbent dose was estimated as 0.2 g/L and it was maintained throughout the experiments. A similar pattern of an inverse relationship between the adsorbent concentration and adsorption capacity was previously reported [39, 40].

3.2.3 Effect of contact time and initial concentration on adsorption capacity

The uptake of any pollutant is highly dependent upon its initial concentration in the aqueous medium. The adsorption capacity of biosorbent as a function of contact time with two different initial dye concentrations (20 mg/L and 40 mg/L) is shown in Fig. 7.

It was observed that the rate of uptake was quick in the beginning up to 10 min and becomes steady thereafter and finally adsorption equilibrium was attained within 10 min. The higher availability of active binding sites on the biosorbent surface for the dye molecules resulted in a faster rate of uptake in the beginning which get saturated in due course of time and uptake slows down in later stages. It was also observed that the adsorption capacity of biosorbent was higher for increased dye concentration (40 mg/L) that may be due to the utilization of all the accessible binding sites for adsorption at higher initial dye concentration [38]. Also, fast kinetics was recorded such that about 26.05 mg/g and 63.16 mg/g of the maximum biosorption capacity obtained

at 20 and 40 mg/L initial dye concentration, respectively was achieved within the first 10 min.
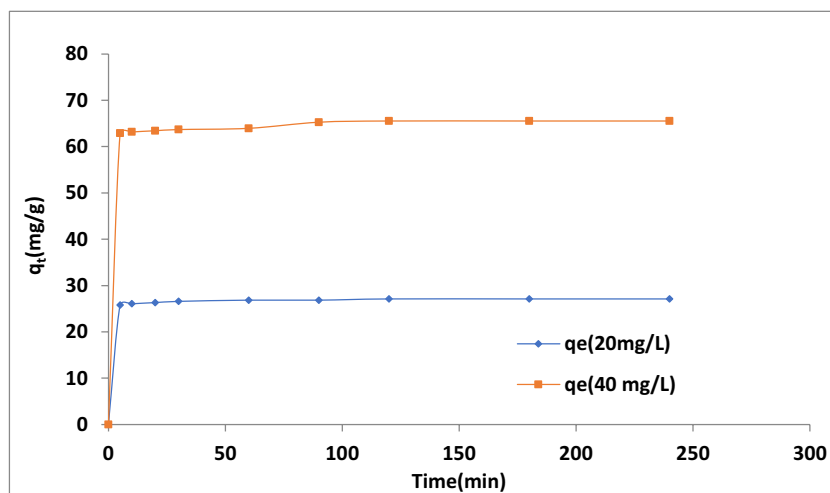
3.2.4 Effect of temperature on adsorption capacity

To examine the effect of temperature on the adsorption capacity of biosorbent, the experiment was performed in different temperature zones from 30 to 70 °C with an initial AV 90 dye concentration of 20 mg/L and keeping other experimental conditions constant (Fig. 8).

It was observed that the AV 90 dye uptake on the biosorbent declines with the rise in temperature suggesting the exothermic nature of the uptake process. This trend can be accounted for by the fact that higher temperature weakens the vander Waals' force and the H-bonding between the adsorbate and the adsorbent resulting in decreased interaction and thus decreased uptake. For the present system, the maximum uptake of AV 90 onto *Zingiber officinale* biosorbent was achieved at 30 °C. Similar findings were also reported by other research groups that low temperatures favored the uptake of the dye onto various materials [38, 41].

3.3 Thermodynamic analysis for uptake of AV 90 onto Zingiber officinale biosorbent

In order to explore the nature and feasibility of uptake of AV 90 dye onto *Zingiber officinale* biosorbent, thermodynamic parameters viz., Gibb's free energy change ($\Delta G°$), enthalpy change ($\Delta H°$) and entropy change ($\Delta S°$) were determined at various pre-defined temperatures. The Gibb's free energy change, $\Delta G°$ was calculated using Eq. (3), the equilibrium constant was estimated by Eq. (4), and the values of enthalpy change, $\Delta H°$ and entropy change, $\Delta S°$ of the adsorption process was determined from the slope and intercept of the Van't Hoff plot Eq. (5) [42, 43].

Fig. 7 Effect of contact time and initial dye concentration on adsorption capacity of *Zingiber officinale* biosorbent for AV 90 dye (reaction conditions: adsorbent conc. = 0.2 g/L; pH = 2; temperature= 30 °C; particle size range= 50−125 μm)

Fig. 8 Effect of temperature on adsorption capacity of *Zingiber officinale* biosorbent for AV 90 dye (reaction conditions: dye conc. = 20 mg/L; adsorbent conc. = 0.2 g/L; pH = 2; particle size range= 50−125 μm)
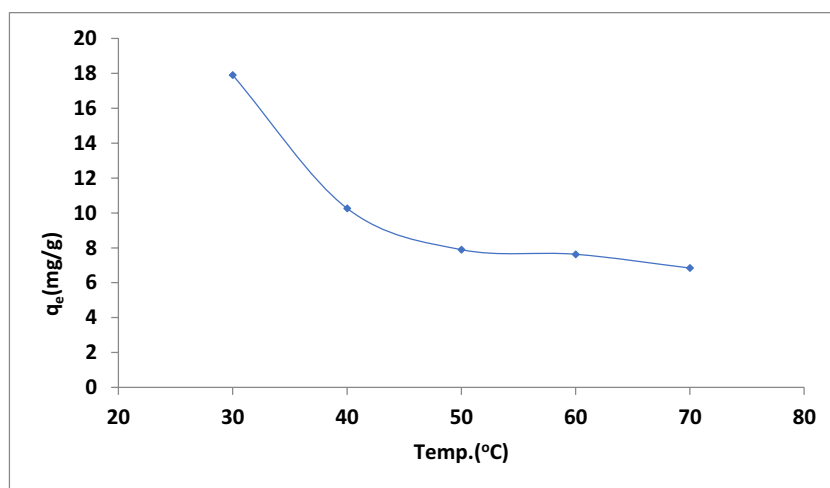
Table 3 Thermodynamic parameters for adsorption of AV 90 dye onto *Zingiber officinale* biosorbent at different temperatures

Temp. (K)	ΔG^o (kJ/mol)	ΔH^o (kJ/mol)	ΔS^o (J/K/mol)
303	−27.56	−409.59	−47.42
313	−26.21		
323	−26.34		
333	−27.01		

$$\Delta G^{\circ} = -RT \ln K^{\circ}_e \tag{3}$$

$$K^0_e = \frac{1000 \times K_L \times Molecular\ Weight\ of\ the\ Adsorbate \times [Adsorbate]^0}{\gamma} \tag{4}$$

$$\ln K^0_e = \frac{\Delta S^0}{R} - \frac{\Delta H^0}{RT} \tag{5}$$

where, K^0_e is the thermodynamic equilibrium constant, $[Adsorbate]^0$ is the standard concentration of adsorbate in mol/L, γ is the activity coefficient, K_L is K of best-fitted isotherm model, T is the absolute temperature in K and R is the universal gas constant (8.314 J/mol K). The thermodynamic parameters and their corresponding values are tabulated in Table 3.

The negative values of ΔG° at all the temperatures confirmed the feasibility and spontaneity of the uptake process of AV 90 dye onto *Zingiber officinale* biosorbent. The negative value of ΔH° (−409.59 kJ/mol) indicated the exothermic nature of the uptake process. The negative value of ΔS° (−47.42 J/K/mol) indicated the good affinity of AV 90 dye molecules towards the *Zingiber* biosorbent and increased disorderness on the biosorbent surface after the uptake process. The findings reported in this study were also

supported by other research groups for the removal of dyes with various materials [44, 45].

3.4 Adsorption isotherms modeling for uptake of AV 90 onto Zingiber officinale biosorbent

Adsorption isotherms explain the forces governing the interaction between the adsorbate and the adsorbent and therefore play an important role in designing any adsorption system. The equilibrium data of the uptake process of AV 90 onto Zingiber biosorbent was analyzed with two parameter isotherms viz., Langmuir, Freundlich, and Tempkin; and three-parameter isotherms viz., Sips and Toth isotherm models to get the most appropriate model explaining the equilibrium data [45].

3.4.1 Langmuir isotherm model

It describes the monolayer adsorption of adsorbate on the surface of adsorbent at finite active sites without having any sort of interaction amid adsorbed molecules. Once the saturation is reached, no further adsorption takes place [46, 47]. The non-linear form of the Langmuir equation is as follows:

$$q_e = \frac{q_0 b C_e}{(1 + b C_e)} \tag{6}$$

where, q_e is the amount of dye adsorbed onto *Zingiber officinale* biosorbent at equilibrium (mg/g) and C_e is the equilibrium concentration of dye in the solution (mg/L), q_0 (maximum adsorption capacity; mg/g) and b (adsorption energy; L/mg) are Langmuir constants.

The values of the Langmuir isotherm constant, a_L (l/mg), and the Langmuir constant, K_L (l/g) are 0.034 and 11.,

respectively indicating a reasonable adsorbent-adsorbate interaction [40, 41].

3.4.2 Freundlich isotherm model

It describes the multilayer adsorption of adsorbate over the heterogenous surface of adsorbent having the non-uniform distribution of heat of adsorption [48]. The non-linear Freundlich equation is used in the following form:

$$q_e = K_f C_e^{1/n} \tag{7}$$

where, q_e is the amount of dye adsorbed onto *Zingiber officinale* biosorbent at equilibrium (mg/g) and C_e is the equilibrium concentration of dye in the solution (mg/L), K_f (adsorption capacity of the adsorbent; mg/g $(L/mg)^{1/n}$ and n (energy of adsorption; g/L) are Freundlich constants.

The value of n, was 1.55, indicating that the adsorption of acid violet 90 ions onto *Zingiber officinale* is favorable; however, a value of 1/n < 1 suggests a slight suppression of adsorption at lower equilibrium concentrations.

3.4.3 Sips isotherm model

This model is a combination of the Langmuir and the Freundlich isotherm models and is expected to effectively explain the heterogeneous surfaces. Based on the concentration of the adsorbent it takes up the form of either of the two models. At low concentrations, it follows Freundlich isotherm, whereas, it reduces to Langmuir isotherm at higher concentrations. The non-linear form of the equation is given as [49, 50]:

$$q_e = \frac{q_m (K_S C_e)^{m_s}}{1 + (K_S C_e)^{m_s}} \tag{8}$$

where, q_e is the amount of adsorbed onto *Zingiber officinale* biosorbent at equilibrium (mg/g) and C_e is the equilibrium concentration of dye in the solution (mg/L), q_m is the maximum adsorption capacity (mg/g), K_S is the Sips equilibrium constant related to adsorption energy and m_s is Sips model exponent characterizing the heterogeneity of the system.

3.4.4 Toth isotherm model

It is useful in describing the adsorption processes in heterogeneous systems. This model assumes that the most of the adsorption sites on the surface of the adsorbent have less adsorption energy than the maximum adsorption energy [50, 51].

$$q_e = \frac{q_T K_T C_e}{\left[\left(1 + K_T C_e \right)^{\beta} \right]^{1/\beta}} \tag{9}$$

where, q_e is the amount of dye adsorbed onto *Zingiber officinale* biosorbent at equilibrium (mg/g) and C_e is the equilibrium concentration of dye in the solution (mg/L), q_T (the maximum monolayer adsorption capacity; (mg/g) and K_T (the adsorption energy; L/mg) are the Toth constants.

The comparison between experimental isotherm data and the theoretical non-linear fitting of isotherm plots for two parameter isotherms (Langmuir, Freundlich, and Tempkin); and three-parameter isotherms (Sips and Toth) for the uptake of AV 90 dye onto the *Zingiber* biosorbent are shown in Fig. 9(a–b). The estimated values of two and three isotherm parameters coupled with their coefficient of determination and error functions with the least normalized sum are depicted in Table 4.
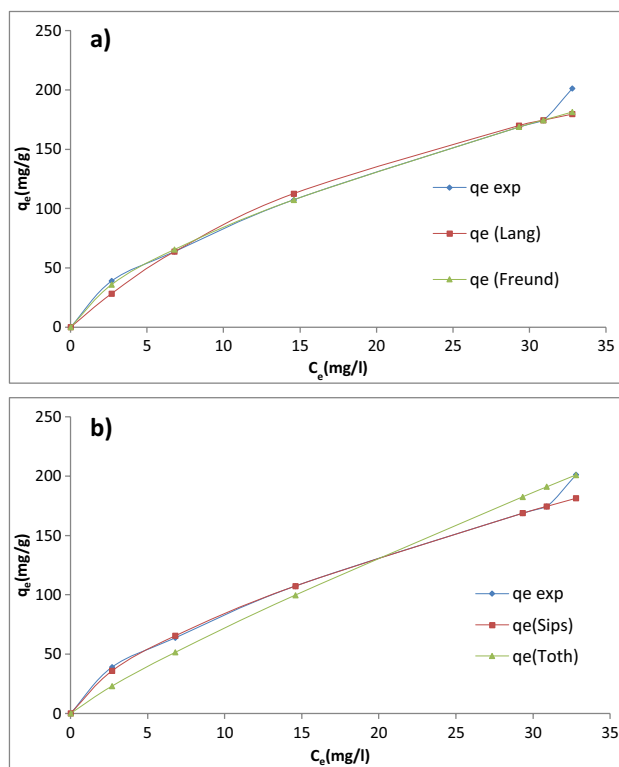
Fig. 9 Comparison between **a** two-parameter models and experimental data and **b** three-parameter models and experimental data obtained for adsorption of AV 90 onto *Zingiber officinale* biosorbent (reaction conditions: adsorbent conc. = 0.2 g/L; pH = 2; temperature= 30 °C; particle size range= 50−125 μm)

Table 4 Isotherm constants and error analysis of two-parameter models for the adsorption of AV 90 dye onto *Zingiber officinale* biosorbent at 30 °C

Isotherm model	Parameter	Value	Error analysis	Value
Langmuir	a_L	0.033572426	ARE	0.437148613
	q_{max}	342.6879035	APE%	7.285810213
	k_L	11.50486414	EABS	38.71458197
			ERRSQ	603.5580181
			Hybrid	5.457228407
			MPSD	0.08819919
			χ^2	6.80517657
			R^2	0.994902011
			SNE	1.097403
Freundlich	n	1.546269689	ARE	0.203840425
	K_F	18.97901166	APE%	3.397340418
			EABS	24.55179932
			ERRSQ	400.3867955
			Hybrid	2.213839394
			MPSD	0.01636864
			χ^2	2.441461763
			R^2	0.996550497
			SNE	1.081982

3.5 Adsorption kinetics for uptake of AV 90 dye onto Zingiber officinale biosorbent

The kinetic analysis of any uptake process furnishes information regarding the rate-determining pathway (chemical reaction, diffusion, and mass transfer), the surface adsorption rate of the adsorbate to the adsorbent, the quantity of species adsorbed (adsorption capacity) and its applicability at industrial scale. The kinetic equations, pseudo-first-order (PFO), pseudo-second-order (PSO), intra-particle diffusion model, and Bangham model were applied to the experimental kinetic data to get the best fit kinetic model [52–54].

3.5.1 Pseudo-first-order and pseudo-second-order kinetic models

The pseudo-first-order model assumes the kinetics of the adsorption process to be physical in nature and diffusion-controlled whereas, the pseudo-second-order model assumes that the rate of adsorption is chemical in nature i.e., controlled by sharing of electrons between the adsorbate and the adsorbent [55].

Then on-linear expressions for pseudo-first-order and pseudo-second-order are outlined as follows:

$$q_t = q_e\left(1 - \exp\left(-k_1 t\right)\right) \tag{10}$$

$$q_t = \frac{k_2 q_e^2 t}{1} + k_2 q_e^t \tag{11}$$

where, q_e and q_t (mg/g) are the amounts of dye adsorbed on *Zingiber* biosorbent at equilibrium and at any time, t, respectively, k_1 (min^{-1}) and k_2 (g/mg/min) are rate constants of pseudo-first-order and pseudo-second-order model equations.

It is clear from the data in Table 5 that the pseudo-first-order and pseudo-second-order models suitably described the kinetic data at both initial dye concentrations. Upon further inspection, it is found that the values of the rate constants (k_1 and k_2) for both models decrease with increasing dye concentration. According to Hameed and Khairy [56], the larger the rate constant, the shorter the time required to attain a fractional uptake within the biosorption system. Hence, the attainment of specific fractional uptake was faster in 20 mg/L than in the 40 mg/L initial dye concentration system in both models. In this regard, two opposing effects can be safely opined regarding an increasing initial dye concentration, namely, the higher the initial concentration, the more the competition between the dye molecules for vacant sites, and the better the rate of solute mass transfer across the biosorbent interface.

3.5.2 Intraparticle diffusion kinetic model

The determination of the rate controlling/determining step in the uptake process improves the understanding of the mechanism

Table 5 Isotherm constants and error analysis of three-parameter models for the adsorption of AV 90 dye onto *Zingiber officinale* biosorbent at 30 °C

Isotherm model	Parameter	Value	Error analysis	Value
Sips	k_S	18.84868477	ARE	0.206339431
	α_S	0.000999774	APE%	3.438990511
	β_S	0.651418656	EABS	24.62823747
			ERRSQ	402.0475247
			Hybrid	2.237691832
			MPSD	0.016921407
			χ^2	2.469524443
			R^2	0.996536284
			SNE	1.082074
Toth	k_τ	9.845909915	ARE	0.847961905
	α_τ	0.078707716	APE%	14.13269842
	$1/\tau$	0.135615238	EABS	66.06214354
			ERRSQ	923.1588335
			Hybrid	12.07918425
			MPSD	0.224543344
			χ^2	16.95630719
			R^2	0.993123526
			SNE	1.119484

involved in the adsorption of adsorbate by the adsorbent. In any adsorption process there are three definite steps that describe the rate (1) intraparticle or pore diffusion, where adsorbate molecules diffused into the interior of the adsorbent, (2) liquid film or surface diffusion, where the adsorbate is transported from the bulk solution to the external surface of the adsorbent, and (3) adsorption on the interior sites of the sorbent. Thus, the kinetic data of the experiments were also analyzed by the intraparticle diffusion model as follows [53, 55]:

$$q_t = k_{id}t^{0.5} + C \qquad (12)$$

where, q_t is the adsorption capacity at any time, t (min), C (mg/g) is the intraparticle diffusion constant related to the boundary layer thickness and k_{id} is the diffusion rate constant (mg/g min$^{1/2}$). The regression of q_t versus $t^{0.5}$ was not linear and did not pass through the origin shows that intraparticle diffusion is not the sole rate-determining step (Fig. 10). Probably, some other mechanisms such as surface as well as external diffusion are responsible for the uptake of AV 90 dye onto *Zingiber officinale* biosorbent.

3.5.3 Bangham kinetic model

To evaluate the possibility of adsorption to be pore-diffusion controlled the kinetic data was analyzed with Bangham's pore diffusion model [50, 54]:

$$q_t = q_e\left[1 - \exp\left(-k_bt^n\right)\right] \qquad (13)$$

where, q_e and q_t (mg/g) are the amounts of dye adsorbed on *Zingiber officinale* biosorbent at equilibrium and at any time, t, respectively, k_b and n are constants.

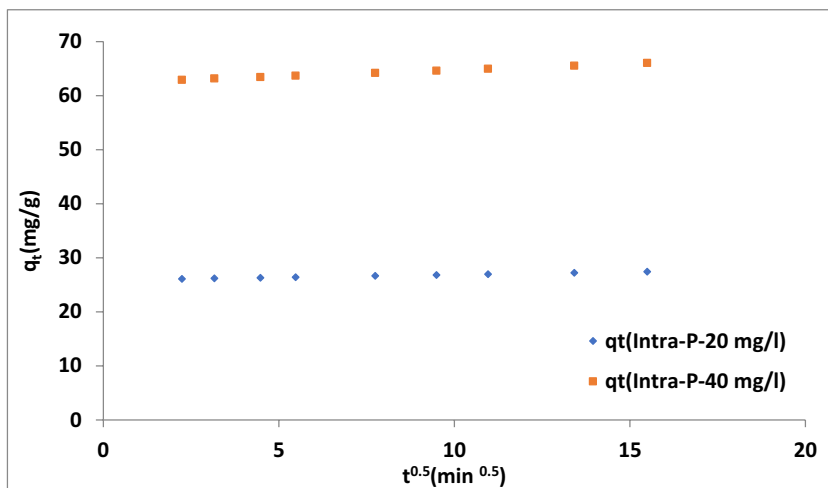The comparison between experimental kinetic data and the theoretical non-linear fitting of kinetic plots for the uptake of AV 90 dye onto the *Zingiber officinale* biosorbent is shown in Fig. 11. The values of estimated kinetic parameters coupled with their coefficient of determination and error functions with the least normalized sum are tabulated in Table 6.

3.6 Statistical validity of the isotherm and kinetic models

3.6.1 Error analysis

The assessment of best-fit isotherm and kinetic models based on linear regression analysis of experimental data is although the most feasible tool but is associated with inherent biasness. It is also inappropriate for isotherm models having more than two parameters. Hence, the non-linear regression analysis of the experimental data and the data obtained from predicted models is done. This method of analysis employed the error analysis using the solver add-in of Microsoft Excel [52, 54, 57]. During error analysis, the error distribution between the experimental data and the data obtained from predicted isotherm and kinetic models was minimized using error functions to determine the most accurate model for isotherm and kinetic data for this study. In this study, to optimize the isotherm and kinetic parameters the common error functions used were: Average relative error (ARE), Average percentage error (APE%), Sum of Absolute Error(EABS), Sum of Squares of Error (ERRSQ/SSE), Hybrid fractional error function (HYBRID), Marquardt's Percent Standard Deviation (MPSD) and Nonlinear chi-square test (χ2) (Table 7). The best-fit isotherm model is selected on the basis of a higher coefficient of regression (R^2) and lower error function values while for the best-fit kinetic model, the closeness between experimental and theoretical q_e values is also considered [54, 57–62].

Fig. 10 Comparison between intra-particle model and experimental data obtained for adsorption of AV 90 onto *Zingiber officinale* biosorbent (reaction conditions: adsorbent conc. = 0.2 g/L; pH = 2; temperature= 30 °C; particle size range= 50–125 μm])
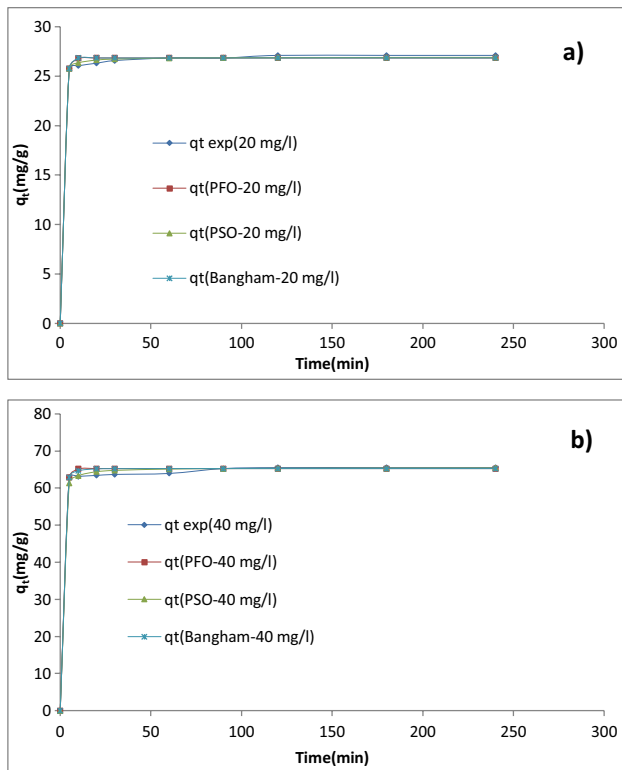
Fig. 11 Comparison between kinetic models and experimental data for adsorption of AV 90 onto *Zingiber officinale* biosorbent (reaction conditions: dye conc.= 20 and 40 mg/L; adsorbent conc. = 0.2 g/L; pH = 2; temperature= 30 °C; particle size range= 50−125 μm)

3.6.2 Best fit isotherm model

Upon non-linear regression analysis of all the isotherm models namely Langmuir, Freundlich, Sips, and Toth, the experimental data were best fitted to the Freundlich isotherm model. The value of n in the Freundlich model (Table 4) is 1.546, satisfying the condition of favorable adsorption (i.e., $0 < n < 10$). Also, it shows the highest R^2 value, as well as the lowest error functions values (Tables 4 and 5) indicating that it gave the best overall fit to the data explaining the equilibrium adsorption of AV 90 dye onto *Zingiber officinale* biosorbent. Based on the correlation coefficient (R^2) and error function values considered in this study, the four isotherm models applied to the experimental data in this study followed the following order of fitness: Freundlich > Sips > Langmuir > Toth.

3.6.3 Best fit kinetic model

The non-linear regression analysis of the kinetic data of AV 90 dye uptake onto *Zingiber* biosorbent was done using four models namely, pseudo-first-order, pseudo-second-order, intraparticle diffusion, and Bangham. According to the results summarized in Table 6, the correlation coefficient of

Table 6 Kinetic model constants and error analysis for adsorption of AV 90 dye onto *Zingiber officinale* biosorbent

Parameter/error analysis	C_o (mg/L)	
	20	40
Pseudo-first-order		
q_e	26.84208533	65.26181051
K_1	0.647740015	0.662918001
ARE	0.087745	0.118509
APE %	0.974944	1.316763
EABS	2.327123	7.550362
ERRSQ	1.113717	11.88553
Hybrid	0.04228	0.187182
MPSD	0.001605	0.002948
χ^2	0.041524	0.182203
R^2	0.999807	0.999651
SNE	4.120381	1.787341
Pseudo second order		
q_e	26.92880916	65.51050816
K_2	0.168113781	0.044750925
ARE	0.053877	0.086223
APE %	0.598629	0.958037
EABS	1.435535	5.483235
ERRSQ	0.347621	6.15967
Hybrid	0.013084	0.097152
MPSD	0.000493	0.001532
χ^2	0.013035	0.097193
R^2	0.999939	0.999817
SNE	7.083214	2.091515
Intra-particle diffusion		
ki_d	0.102358009	0.23361068
C	25.85798133	62.39209132
ARE	0.051914	0.031375
APE %	0.576821	0.348614
EABS	1.381574	2.044261
ERRSQ	0.313841	1.060876
Hybrid	0.011802	0.016242
MPSD	0.000444	0.000249
χ^2	0.011723	0.016323
R^2	0.999945	0.999968
SNE	7.481875	3.316071
Bangham model		
q_e	26.84209372	65.26377665
k_b	0.041474101	1.482903737
n	2.707687051	0.5
ARE	0.089331	0.108649
APE %	0.992568	1.207212
EABS	2.368446	6.926959
ERRSQ	1.177267	9.72604
Hybrid	0.044719	0.153018
MPSD	0.001699	0.002407
χ^2	0.043859	0.149423
R^2	0.999796	0.999714
SNE	4.007493	1.878844

Table 7 List of non-linear error functions used in this study

Error function	Equation	References
Average relative error (ARE)	$ARE = \sum_{i=1}^{n} \left\lvert \frac{(q_e)_{exp.} - (q_e)_{calc.}}{(q_e)_{exp.}} \right\rvert$	[58]
Average percentage error (APE)	$APE\% = \frac{\sum_{i=1}^{N} \left\lvert \left[\left((q_e)_{exp.} - (q_e)_{calc.} / q_{exp.} \right) \right] \right\rvert}{N} x100$	[59]
Sum of absolute error (EABS)	$EABS = \sum_{i=1}^{n} \left\lvert q_{e,exp.} - q_{e,calc.} \right\rvert$	[60]
Sum squares error (ERRSQ/SSE)	$ERRSQ = \sum_{i=1}^{n} \left[(q_e)_{calc.} - (q_e)_{exp.} \right]^2$	[55]
Hybrid fraction error function (hybrid)	$Hybrid = \frac{100}{n-p} \sum_{i=1}^{n} \left[\frac{\left((q_e)_{exp.} - (q_e)calc. \right)^2}{(q_e)_{exp.}} \right] i$	[61]
Marquardt's percent standard deviation MPSD	$MPSD = (100 \sqrt{ \frac{1}{n-p} \sum_{i=1}^{n} \left[\frac{\left((q_e)_{exp.} - (q_e)_{calc.} \right)}{(q_e)_{exp.}} \right]^2 }$	[62]
Nonlinear chi-square test(χ^2)	$\chi^2 = \sum \frac{(q_{e.exp} - q_{e.theoretical})^2}{q_{e.theoretical}}$	[46]
Coefficient of determination (R^2)	$R^2 = \frac{\sum_{i=1}^{n} (q_{e,calc} - \overline{q_{e,exp}})^2}{\sum_{i=1}^{n} (q_{e,calc} - \overline{q_{e,exp}})^2 + \sum_{i=1}^{n} (q_{e,calc} - q_{e,exp})^2}$	[45]

all the models is close, but the error function values are quite different indicating a better fitting of experimental data to the kinetic model. On the basis of lower values of error functions and the closeness between calculated and theoretical q_e values, the pseudo-second-order kinetic model provides the best fitting to the experimental data. It indicated that the adsorption of AV 90 dye was chemical in nature, i.e., chemisorption. The overall fitness of the models based on the results summarized in Table 6, the four models can be ordered as pseudo-second-order > Bangham > intraparticle diffusion > pseudo-first-order.

Further, the plot of intraparticle diffusion (Fig. 10) suggested that the adsorption was not controlled by intraparticle diffusion only, instead surface diffusion and external diffusion also participated in the uptake process. The plateau in the plot suggested slow diffusion of adsorbate into the inner pores of the adsorbent. Furthermore, higher R^2 values evaluated from the fitting analysis (Table 5) demonstrated that the uptake process is governed by pore-diffusion. This observation was confirmed by Bangham plot (Fig. 11) where the experimental points are aligned on a line and the correlation coefficient is closer to the unity i.e., (R^2 = 0.997).

3.6.4 Proposed mechanism of uptake of AV 90 dye onto Zingiber officinale biosorbent

Understanding the adsorption mechanism of acid violet 90 onto *Zingiber officinale* makes it easier to remove dyes during wastewater treatment. The removal of acid violet 90 from aqueous solution onto *Zingiber officinale* may be described by two steps; firstly, electrostatic attraction between the positively charged groups of *Zingiber officinale* occurs in solution at optimal pH (4.0) and the negatively charged (-SO3⁻) groups of acid violet 90. The second is the hydrogen bonding between the –OH group of *Zingiber officinale* and the O atom of the acid violet 90 dye molecule. The third is intra-particle diffusion control involving (a) movement of the adsorbate from the bulk solution to the adsorbent surface, (b) diffusion of the adsorbate through the boundary layer to the adsorbent surface, and (c) intra-particle diffusion of the dye molecules into the internal pores of the adsorbent. Finally, pi-pi stacking interactions

Table 8 Comparison of adsorption capacity of *Zingiber officinale* biosorbent with other adsorbents for AV 90 dye

Adsorbent	Adsorption capacity (mg/g)	References
Waste Red Mud	1.37	63
Polyaniline (PANI)	153.85	37
polyaniline/Gördes-clinoptilolite (PANI/GC) composite materials	72.46	37
RHA/PFA/CFA Sorbent	30.74	64
Candida tropicalis yeast	41.3 mg/g	65
Penicillium sp. Biosorbent	4.32	66
Processed Agricultural Waste	167	67
Zingiber officinale	342.69	Present study

3.6.5 Comparison of adsorption capacity of Zingiber officinale biosorbent with other adsorbents for AV 90 dye

The maximum adsorption capacity for acid violet 90 onto *Zingiber officinale*, according to the Langmuir isotherm model, was 342.69 mg g^{-1}. This relatively large adsorption capacity value is an indication of the strong affinity between the *Zingiber officinale* and the acid violet 90 molecules [37, 63–67] as compared to the result of the previous studies which are shown in Table 8.

4 Conclusion

The present study revealed the effectiveness of *Zingiber officinale* biosorbent for the effective uptake of AV 90 dye from an aqueous medium. The operational parameters have influenced the overall adsorption process. The optimum adsorption (342.68 mg/g) was achieved at pH 2, adsorbent dose 0.2 g/L, contact time 10 min, and 40 mg/L dye concentration at a temperature of 30 °C. The thermodynamic parameters $\Delta H°$ (−456.35 kJ/mol), $\Delta S°$ (−58.50 J/K/mol) and $\Delta G°$ (7.83 × 10^{-3} kJ/mol) indicated the exothermic, spontaneous, and feasible process of dye uptake. The isotherm of the process was well explained by Freundlich isotherm model based on the higher R^2 and lower error function values and it followed the order of fitness: Freundlich > Sips > Langmuir > Toth. The pseudo-second-order model best explained the kinetics of the uptake process based on higher R^2 lower error function values and the closeness of calculated and theoretical q$_e$ values. The intraparticle diffusion was not the only rate-determining step, besides Bangham plot suggested the involvement of pore diffusion in the rate-determining step. The chemical nature of adsorption was also supported by the equilibrium time i.e., within 10 min of the process adsorption equilibrium was attained. Based on the adsorption capacity displayed by the *Zingiber officinale* biosorbent it can be concluded that this biosorbent is highly efficient for removal of the AV 90 dye and can be used as an alternative candidate for removing other organic pollutants from aqueous medium.

Author contribution Hashem: conceptualization, project administration, data curation, supervision, writing—original draft, and writing—review and editing. Shikha Dubey: data curation, writing—original draft, and writing—review and editing. Y.C. Sharma data curation, writing—original draft, and writing—review and editing. S. Farag: experimentation, formal analyses, data curation, and writing—review and editing. A.A. Aly: investigation, formal analyses, data curation, and writing—review and editing.

Declarations

Ethics approval Not applicable

Conflict of interest The authors declare no competing interests.

References

1. Hussain T, Wahab A (2018) A critical review of the current water conservation practices in textile wet processing. J Clean Prod 198:806–819. https://doi.org/10.1016/j.jclepro.2018.07.051
2. Kiron MI (2014) Water consumption in textile processing industry. In: Water Consumption in Textile Processing Industry-Textile Learner
3. Samanta KK, Pandit P, Samanta P, Basak P (2019) Water consumption in textile processing and sustainable approaches for its conservation, Water in Textiles and Fashion. Elsevier Ltd. https://doi.org/10.1016/b978-0-08-102633-5.00003-8
4. Roy M, Sen P, Pal P (2020) An integrated green management model to improve environmental performance of textile industry towards sustainability. J Clean Prod 271:122656–122664. https://doi.org/10.1016/j.jclepro.2020.122656
5. Correia VM, Stephenson T, Judd SJ (1994) Characterisation of textile wastewaters – areview. Environ Technol 15:917–929. https://doi.org/10.1080/09593339409385500
6. Taylor P, Bisschops I, Spanjers H (2003) Literature review on textile wastewatercharacterisation. Environ Technol 24(11):1399–1411. https://doi.org/10.1080/09593330309385684
7. Yaseen DA, Scholz M (2019) Textile dye wastewater characteristics and constituents of synthetic effluents: a critical review. Int J Environ Sci Technol 16:1193–1226. https://doi.org/10.1007/s13762-018-2130-z
8. Dai Y, Zhang N, Xing C, Cui Q, Sun Q (2019) The adsorption, regeneration and engineering applications of biochar for removal organic pollutants: a review. Chemosphere 223:12–27. https://doi.org/10.1016/j.chemosphere.2019.01.161
9. Saghir S, Pu C, Fu E, Wang Y, Xiao Z (2022) Synthesis of high surface area porous biochar obtained from pistachio shells for the efficient adsorption of organic dyes from polluted water. Surf Interfaces 34:102357. https://doi.org/10.1016/j.surfin.2022.102357

10. Boysan F (2021) Removal of acid violet 90 Dyestuffs in aqueous solutions by ozonation method. Sak Univ J Sci 25:200–211. https://doi.org/10.16984/saufenbilder.830702

11. Chung KT (2016) Azo dyes and human health: a review. Environ Sci Heal Care 34(4):233–261. https://doi.org/10.1080/10590501.2016.1236602

12. Hashem A, Aniagor CO, Morsy OM, Abou-Okeil A, Aly AA Apricot seed shell: an agro-waste biosorbent for acid blue193 dye adsorption. Biomass Conv Bioref:1–4. https://doi.org/10.1007/s13399-022-03272-9

13. Lellis B, Fávaro-Polonio CZ, Pamphile JA, Polonio JC (2019) Effects of textile dyes on health and the environment and bioremediation potential of living organisms. Biotechnol Res Innov 3:275–290. https://doi.org/10.1016/j.biori.2019.09.001

14. Bafana A, Devi SS, Chakrabarti T (2011) Azo dyes: past, present and the future. Environ Rev 19:350–370. https://doi.org/10.1139/a11-018

15. Rathi BS, Senthil Kumar P (2022) Sustainable approach on the biodegradation of azo dyes: a short review. Curr Opin Green Sustain Chem 33:100578. https://doi.org/10.1016/j.cogsc.2021.100578

16. Hernández-Montoya V, Pérez-Cruz MA, Mendoza-Castillo DI, Moreno-Virgen MR, Bonilla-Petriciolet A (2013) Competitive adsorption of dyes and heavy metals on zeolitic structures. J Environ Manag 116:213–221. https://doi.org/10.1016/j.jenvman.2012.12.010

17. Iqbal MJ, Ashiq MN (2007) Adsorption of dyes from aqueous solutions on activated charcoal. J Hazard Mater 139:57–66. https://doi.org/10.1016/j.jhazmat.2006.06.007

18. Visa M, Bogatu C, Duta A (2010) Simultaneous adsorption of dyes and heavy metals from multicomponent solutions using fly ash. Appl Surf Sci 256:5486–5491. https://doi.org/10.1016/j.apsusc.2009.12.145

19. Zhao X, Zhu H, Chen J, Ao Q (2015) FTIR, XRD and SEM analysis of ginger powderswith different size. J Food Process Preserv 39(6):2017–2026. https://doi.org/10.1111/jfpp.12442

20. Bilal M, Ihsanullah I, Shah MUIH, Reddy AVB, Aminabhavi TM (2022) Recent advances in the removal of dyes from wastewater using low-cost adsorbents: a review. J Environ Manage 321:115981. https://doi.org/10.1016/j.jenvman.2022.115981

21. El-Ghorab AH, Nauman M, Anjum FM, Hussain S, Nadeem M (2010) A comparative study on chemical compositionand antioxidant activity of Z. officinale (Zingiber officinale) and Cumin (Cuminum cyminum). J Agric Food Chem 58:8231–8237. https://doi.org/10.1021/jf101202x

22. Kumar R, Ahmad R (2011) Biosorption of hazardous crystal violet dye from aqueous solution onto treated ginger waste (TGW). Desalin 265:112–118. https://doi.org/10.1016/j.desal.2010.07.040

23. Barman K, Chowdhury D, Baruah PK (2019) Biosynthesized silver nanoparticles using Zingiber officinale rhizome extract as efficient catalystfor the degradation of environmental pollutants. Inorg Nano-Met Chem 50(2):57–65. https://doi.org/10.1080/24701556.2019.1661468

24. Buvaneswari K, Singanan M (2022) Removal of malachite green dye in synthetic wastewater using zingiber officinale plant leaves biocarbon. Mater Today 55:274–279. https://doi.org/10.1016/j.matpr.2021.07.137

25. Ahmad R, Kumar R (2010) Adsorption studies of hazardous malachite green onto treated ginger waste. J Environ Manage 91(4):1032–1038. https://doi.org/10.1016/j.jenvman.2009.12.016

26. Karthickeyan V (2018) Effect of nature based antioxidant from Zingiber officinale Rosc. on the oxidation stability, engine performance and emission characteristics with neem oil methyl ester. Heat Mass Transf 54:3409–3420. https://doi.org/10.1007/s00231-018-2380-9

27. Hashem A, Aniagor CO, Nasr MF, Abou-Okeil A (2021) Efficacy of treated sodium alginate and activated carbon fibre for Pb (II) adsorption. Int J Biol Macromol 176:201–216

28. Markam R, Bajpai J, Bajpai AK (2019) Synthesis of ginger derived nanocarriers (GDNC) and study of in vitro release of 5-amino salicylic acid (5-ASA) as an anti inflammatory drug. J Drug Deliv Sci Technol 50:355–364. https://doi.org/10.1016/j.jddst.2019.01.039

29. Hashem A, Ahmad F, Fahad R (2008) Application of some starch hydrogels for the removal of mercury(II) ions from aqueous solutions. Adsorp Sci Technol 26(8):563–579

30. Hashem A, Aniagor CO, Abdel-Halim ES, Amr A, Farag S, Aly AA (2022) Instrumental characteristics and acid blue 193 dye sorption properties of novel lupine seed powder. CLCE 2:100011

31. Zhang L, Xie W, Zhao X, Liu Y, Gao W (2009) Study on the morphology, crystalline structure and thermal properties of yellowginger starch acetates with different degrees of substitution. Thermochimica Acta 495:57–62

32. Sousa IR, Alves RJ, Corrêa AC, de Campos Pastre A, Luchesi BR, Marconcini JM, Bondância TJ, Corradini E, Stefani R, de Morais Teixeira E (2020) Structural, morphological and thermal characterization of ginger starch (zingiberofficinale) isolated from rhizome. Revista Panorâmica online – ISSN 2238-9210 Edição Especial

33. Collona P, Buleon A, Mercier C (1987) Starch: properties and potential. In: Galliard T (ed) Volume 13 of Critical Reports on Applied Chemistry. Published for the Society of Chemical Industry by John Wily & Sons, Chichester ISBN 0-471-91326-X.

34. Xu Y, Miladinov V, Hanna MA (2004) Synthesis and characterization of starch acetates with high substitution1. Cereal Chem 81:735–740

35. Menkiti M, Aniagor CO, Onuzulike CM, Ejimofor MI, Okonkwo SS (2022) Chromium adsorption from petroleum refinery wastewater using biocomposites. Results in Surfaces and Interfaces 8:100064

36. Rápó E, Tonk S (2021) Factors affecting synthetic dye adsorption; desorption studies: a review of results from the last five years (2017–2021). Molecules 26(17):5419

37. Akti F, Okur M (2018) The removal of acid violet 90 from aqueous solutions using PANI and PANI/clinoptilolite composites: isotherm and kinetics. J Polym Environ 26:4233–4242. https://doi.org/10.1007/s10924-018-1297-1

38. Noreen S, Bhatti HN, Iqbal M, Hussain F, Sarim FM (2020) Chitosan, starch, polyaniline and polypyrrolebiocomposite with sugarcane bagasse for the efficient removal of Acid Black dye. Int J BiolMacromol 147:439–452. https://doi.org/10.1016/j.ijbiomac.2019.12.257

39. Jain SN, Shaikh Z, Mane VS, Vishnoi S, Mawal VN, Patel OR, Bhandari PS, Gaikwad MS (2019) Nonlinear regression approach for acid dye remediation using activated adsorbent: kinetic, isotherm, thermodynamic and reusability studies. Microchem J 148:605–615

40. Ahmadi S, Mohammadi L, Rahdar A, Rahdar S, Dehghani R, Adaobi Igwegbe C, Kyzas GZ (2020) Acid dye removal from aqueous solution by using neodymium (III) oxide nanoadsorbents. Nanomater 10(3):556

41. Maqbool M, Sadaf S, Bhatti HN, Rehmat S, Kausar A, Alissa SA, Iqbal M (2021) Sodium alginate and polypyrrole composites with algal dead biomass for the adsorption of Congo red dye: kinetics, thermodynamics and desorption studies. Surf Interfaces 25:101183. https://doi.org/10.1016/j.surfin.2021.101183

42. Işık B, Kurtoğlu AE, Gürdağ G, Keçeli G (2021) Radioactive cesium ion removal from wastewater using polymer metal oxide composites. J Hazard Mater 403:123652. https://doi.org/10.1016/j.jhazmat.2020.123652

43. Lima EC, Bandegharaei AH, Moreno-Piraján JC, Anastopoulos I (2018) A critical review of the estimation of thethermodynamic parameters on adsorption equilibria. Wrong use of equilibrium constantin the Van't Hoof equation for calculation of thermodynamic parameters of adsorption. J Mol Liq 273:425–434. https://doi.org/10.1016/j.molliq.2018.10.048

44. Bhatti HN, Safa Y, Yakout SM, Shair OH, Iqbal M, Nazir A (2020) Efficient removal of dyes using carboxymethyl cellulose/alginate/polyvinyl alcohol/rice husk composite: adsorption/desorption, kinetics and recycling studies. Int J Biol Macromol 150:861–870. https://doi.org/10.1016/j.ijbiomac.2020.02.093

45. Vijayaraghavan K, Padmesh TVN, Palanivelu K, Velan M (2006) Biosorption of nickel(II) ions onto *Sargassum wightii*: application of two-parameter and three-parameter isotherm models. J Hazard Mater 133:304–308. https://doi.org/10.1016/j.jhazmat.2005.10.016

46. Boulinguiez B, Cloirec PL, Wolbert D (2008) Revisiting the determination of Langmuir parameters application to tetrahydrothiophene adsorption onto activated carbon. Langmuir 24:6420–6424. https://doi.org/10.1021/la800725s

47. Langmuir I (1916) The constitution and fundamental properties of solids and liquids. Part I. solids. J Am Chem Soc 38:2221–2295. https://doi.org/10.1021/ja02254a006

48. Freundlich H (1907) Über die adsorption in lösungen. Zeitschrift fur Physikalische Chemie-Leipzig 57:385–470. https://doi.org/10.1515/zpch-1907-5723

49. Sips R (1948) On the structure of a catalyst surface. J Chem Phys 16:490–495. https://doi.org/10.1063/1.1746922

50. Hashem A, Hussein HA, Sanousy MA, Adam E, Saad EE(2011) Monomethylolated Thiourea - Sawdust as a New Adsorbent for Removal of Hg (II) from Contaminated Water: Equilibrium Kinetic and Thermodynamic Studies. Polym Plast Technol Eng 50(12) 1220–1230.

51. Toth J (1971) State equation of the solid-gas interface layers. Acta chim hung 69:311–317

52. Kajjumba GW, Emik S, Öngen A, Özcan HK, Aydın S (2018) Modelling of adsorption kinetic processes—errors, theory and application. In: Advanced Sorption Process Applications. Intech Open, pp 1–19. https://doi.org/10.5772/intechopen.80495

53. Aniagor CO, Igwegbe CA, Ighalo JO, Oba SN (2021) Adsorption of doxycycline from aqueous media: a review. J Mol Liq 334:116124. https://doi.org/10.1016/j.molliq.2021.116124

54. Dada AO, Adekola FA, Odebunmi EO, Odebunmi AS, Ogunlaja AS, Bello OS (2021) Two–three parameters isotherm modeling, kinetics with statistical validity, desorption and thermodynamic studies of adsorption of Cu(II) ions onto zerovalent iron nanoparticles. Sci Rep 11:16454. https://doi.org/10.1038/s41598-021-95090-8

55. Kumar KV, Sivanesan S (2006) Pseudo second order kinetics and pseudo isotherms for malachite green onto activated carbon: comparison of linear and nonlinear regression methods. J Hazard Mater B 136:721–726. https://doi.org/10.1016/j.jhazmat.2006.01.003

56. Hameed B, El-Khaiary M (2008) Removal of basic dye from aqueous medium using a novel agricultural waste material: Pumpkin seed hull. J Hazard Mater 155(3):601–609

57. Dubey S, Gusain D, Sharma YC (2016) Kinetic and isotherm parameter determination for the removal of chromium from aqueous solutions by nanoalumina, a nanoadsorbent. J Mol Liq 21:1–8. https://doi.org/10.1016/j.molliq.2016.01.021

58. Kapoor A, Yang RT (1989) Correlation of equilibrium adsorption data of condensable vapours on porous adsorbents. Gas Sep Purif 3:187–192. https://doi.org/10.1016/0950-4214(89)80004-0

59. Rangabhashiyam S, Anu N, Nandagopal M (2014) Relevance of isotherm models in biosorption of pollutants by agricultural byproducts. J Env Chem Eng 2(1):398–414. https://doi.org/10.1016/j.jece.2014.01.014

60. Hashem A, Fletcher AJ, El-Sakhawy M, Mohamed LA, Farag S (2020) Aminated hydroximoyl camelthorn residues as a novel adsorbent for extracting Hg(II) from contaminated water: studies of isotherm, kinetics, and mechanism. J Polym Environ 28(9):2498–2510

61. Hashem A, Aniagor CO, Hussein DM, Farag S (2021) Application of novel butane-1,4-dioic acid-functionalized cellulosic biosorbent for aqueous cobalt ion sequestration. Cellulose 28(6):3599–3615

62. Marquardt DW (1963) An algorithm for least-squares estimation of nonlinear parameters. J Soc Ind Appl Math 11:431–441. https://doi.org/10.1137/0111030

63. Namasivayam C, Yamuna RT, Arasi DJSE (2001) Removal of acid violet from wastewater by adsorption on waste red mud. Environ Geol 41:269–273

64. Dahlan I, Noor ASM (2014) Study on the removal characteristic of acid violet dye from synthetic wastewater using a novel RHA/PFA/CFA SORBENT. Environ Eng Manag J 13(1):197–204. https://doi.org/10.30638/eemj.2014.024

65. Okur M, Saraçoğlu N, Aksu Z (2014) Use of response surface methodology for the bioaccumulation of Violet 90 metal-complex dye by Candida tropicalis. Turkish J Eng Environ Sci 38(2):217–230. https://doi.org/10.3906/muh-1409-2

66. Oblesha A, Santoshkumara M, Nayak A, Karegoudar TB (2009) Biosorption of acid violet dye from aqueous solutions using native biomass of a new isolate of Penicillium sp. Int Biodeterior Biodegradation 63:782–787. https://doi.org/10.1016/j.ibiod.2009.06.005

67. Deshannavara UB, Hegde PG, Patil PS, Tamburi N, Ruchi K, Kolur A, Jadhav A, El-Harbawi M (2021) Adsorption of Acid Violet 49 dye from aqueous solution by processed agricultural waste. Desalin Water Treat 210:415–429